IISc Theses Abstracts

Contents

J. Indian Inst. Sci., May–June 1996, 76, 397–430.

IISc THESES ABSTRACTS

Thesis Abstract (M.Sc. (Engng))
Conjugate mixed convection in vertical parallel plate channels by K. S. Harish
Research supervisors: M. V. Krishnamurthy and M. H. Kori (CDOT)
Department: Mechanical Engineering

1. Introduction

Fans are often used to cool heated parts in electronic equipment. The most commonly occurring situation is a vertical channel made by two adjoining PCBs. In such cases, when the fan velocities are small, mixed convection results. Dalbert[1], Hallinan and Qureshi[2] and Habchi and Acharya[3] studied mixed convection in parallel plate channels. They did not consider the effect of conduction in the plates. On the other hand, studies including the effect of wall conduction are restricted to natural convection; for example, the work of Burch *et al.*[4] This work is an effort to bridge the gap and is a study of aiding and opposing mixed convection in parallel plate channels with isoflux heating, including the effect of wall conduction.

2. Formulation and solution

Conjugate mixed convection in isoflux parallel plate channels with two-dimensional conduction in the walls has been formulated using completely elliptic governing equations without making boundary-layer approximations. Figure 1 shows the model used. Stream function vorticity transformation has been employed. The model has been numerically solved for various values of parameters like Reynolds number and Grashof number. Solutions have been obtained for the

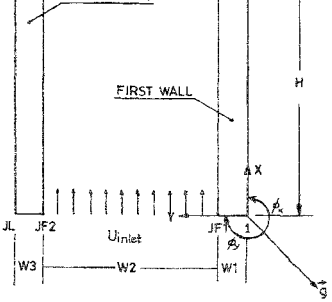

FIG 1. A Channel formed by adjacent circuit boards.

symmetric and asymmetric heating conditions. A thermal diffusivity ratio of 50, aspect ratio of 10, and a Prandtl number of 0.71 have been used. Parametric study by varying the thermal conductivity ratio and nondimensional wall thickness has been done.

3. Results

Temperature profiles have been obtained and plotted at different channel heights. For the symmetrically heated channel the temperature profile has three parts, a decreasing profile in each of the walls and a parabolic trough in the fluid region. In the asymmetrically heated channel the temperature falls monotonically as the distance from the wall increases. In this channel, wall temperatures are lower than for the corresponding symmetric case. Therefore, in the construction of electronic packages, a PCB with an inactive neighbouring PCB is better cooled than a PCB with a heated neighbouring PCB, both heated to the same extent.

Longitudinal fluid velocity profiles have been obtained and plotted at various channel heights. The velocity profile is characterised by a uniform velocity core in the middle and a thin velocity boundary layer near the walls, the thinness increasing with Reynolds number. Near the entry a centreline velocity depression is observed. As the Grashof number increases, the velocity profile becomes more asymmetric with the hump shifting towards the hot wall in aiding flow and towards the cold wall in opposing flow.

Variation of fluid bulk mean temperature, interface heat flux, local Nusselt numbers based both on the fluid bulk mean temperature and the average wall temperature are plotted. The channel average Nusselt number, defined in such a way as to relate directly to the peak temperature in the channel, is computed for each case. Effect of varying parameters like Reynolds number, Grashof number, thermal conductivity ratio and nondimensional wall thickness is studied.

4. Correlations

The Nusselt number for forced convection and the Nusselt number for mixed convection, 'the former being independent of Grashof number', are correlated as functions of Reynolds number, Grashof number, ratio of thermal conductivities and nondimensional wall thickness as given below:

Correlations for forced convection

For symmetric case,

$$Nu_f = 2.06\,\mathrm{Re}^{0.34}\,\lambda_s^{-0.15} w^{-0.41} \tag{1}$$

For asymmetric case,

$$Nu_f = 1.10\,\mathrm{Re}^{0.32}\,\lambda_s^{-0.15} w^{-0.41} \tag{2}$$

Correlations for mixed convection aiding flow

For symmetric case,

$$\frac{Nu_m}{Nu_f} = 1 + 0.0083\left(\frac{Gr}{\mathrm{Re}^2}\right)^{0.75} \lambda_s^{0.33} w^{0.25} \tag{3}$$

For asymmetric case

$$\frac{Nu_m}{Nu_f} = 1 + 0.0075\left(\frac{Gr}{\mathrm{Re}^2}\right)^{0.86} \lambda_s^{0.47} w^{0.43} \tag{4}$$

Correlations for mixed convection opposing flow

For symmetric case,

$$\frac{Nu_m}{Nu_f} = 1 - 0.0076\left(\frac{Gr}{\mathrm{Re}^2}\right)^{1.03} \lambda_s^{0.47} w^{0.38} \tag{5}$$

For asymmetric case,

$$\frac{Nu_m}{Nu_f} = 1 - 0.017\left(\frac{Gr}{\mathrm{Re}^2}\right)^{0.87} \lambda_s^{0.33} w^{0.55}. \tag{6}$$

5. Conclusions

For symmetrically heated channels the temperature profile has three parts, a decreasing profile in each of the two walls and a parabolic trough in the fluid channel. The asymmetrically heated channel is better cooled than the symmetrically heated channel. The local Nusselt numbers are maximum at the entry of the channel. The local Nusselt numbers increase by increasing the Reynolds number. An increase in wall thickness reduces the heat transfer and the cooling effect. Increasing the ratio of thermal conductivities also reduces the heat transfer and Nusselt number. In the parameter range considered, a heat-transfer enhancement of 16% in the symmetric case and 19% in the asymmetric case is recorded in aiding flow. For thin walls, heat-transfer enhancements are 30.76 and 37.6% in aiding flow, symmetric and asymmetric heating conditions, respectively. For high-conductivity ratios, the figures are 42.47 and 54.58%, respectively, and 19.51 and 22.58%, respectively, for low-conductivity ratios. In opposing flow, no heat-transfer enhancement is observed. The Nusselt number for forced convection, and the mixed convection Nusselt number (the former being independent of Grashof number) are correlated as functions of Reynolds number, Grashof number, thermal conductivity ratios and wall thickness.

References

1. D'ALBERT, A. M. — Natural mixed and forced convection in a vertical channel with asymmetric uniform heating, heat transfer 1982, *Proc. Seventh Int. Heat Transfer Conf.*, Munchen, Federal Republic of Germany, Vol. 3, Hemisphere Publishing, pp. 431–434.

2. HALLINAN, K. P. AND QURESHI, Z. H. — Heat transfer enhancement *via* opposing mixed convection in vertical isoflux channels, *ASME HTD*, 1988, **100**, 35–41.

3. HABCHI, S. AND ACHARYA, S. — Laminar mixed convection in a symmetrically or asymmetrically heated vertical channel, *Num Heat Trans.*, 1986, **9**, 605–618.

4. BURCH, R., RHODES, T. AND ACHARYA, S. — Laminar natural convection between finitely conducting vertical plates, *Int. J. Heat Mass Trans.*, 1985, **28**, 1173–1186.

Thesis Abstract (M. Sc. (Engng))

The constitutive flow behaviour of Al 6061–SiC MMCs and related relaxation and restoration mechanisms during hot deformation by Jaydeep Sarkar

Research supervisor: M. K. Surappa

Department: Metallurgy

1. Introduction

Particulate reinforced metal matrix composites (MMCs) are very attractive materials, as they can be manufactured at reasonable cost. Most MMCs are produced in the form of billets which are subsequently subjected to secondary processing such as extrusion, rolling or forging and are currently the subject of considerable attention. While both the fabrication and mechanical properties of particle-reinforced MMCs have been widely investigated, the effect of thermomechanical processing on the microstructure has been less extensively studied. The improved workability stems from dynamic recovery (DRV); however, it is possible that particle-stimulated nucleation (PSN) of dynamic recrystallization (DRX) makes a substantial contribution. Avoidance of microcracks in the particles is also very important for sound products. It is therefore important to understand the effect of thermomechanical processing parameters such as strain, strain rate and temperature on the microstructure of MMCs. Not much information has been published on how the presence of large SiC_p particles of varying sizes and volume per cent influence the restoration processes in SiC_p-reinforced Al 6061 alloy-based MMCs, produced by inexpensive casting routes.

In the present study, the effects of volume per cent and size of SiC particles on the constitutive flow behaviour, relaxation and restoration processes of MMCs have been evaluated. Existing models[1–6] have been used for this purpose and new models have also been proposed which are in good agreement with experimental results.

2. Experimental procedures

An Al 6061 alloy has been used as matrix material for the fabrication of MMCs. SiC_p of average sizes 20 and 40 μm have been selected as reinforcements. The 11 vol. pct 20 and 40 μm SiC_p-reinforced MMCs are designated as A1 1-20 and A1 1-40, respectively. Similarly, 18 vol. pct 40 μm MMC as A1 8-40 in the following sections. Cylindrical compression specimens (15 × 10 mm) are deformed at constant true strain rates ($\dot{\epsilon}$) of 0.001, 0.01, 0.1 and 1.0 s^{-1} over a temperature range of 300°–550°C. Compression tests have been carried out on a computer-controlled servo-hydraulic machine (DARTEC). Processing and instability maps have been developed for MMCs and for unreinforced alloys (A). Referring to these maps, selected specimens are sectioned along the compression axis and subsequently the microstructures are examined both under optical and scanning electron microscopes (SEM).

3. Results and discussion

The true stress *versus* true strain curves of MMCs reveal either steady-state or near steady-state flow behaviour at all combinations of strain rate and temperature. Isothermal true stress values are found to be a strong function of imposed strain rate (Fig. 1). Similar to the unreinforced alloy (A), all MMCs show a rise in true stress value with increase in strain rate at a given temperature. Moreover, the present data show that the true stress values do not change appreciably with changing volume per cent and size of SiC particles. It has been observed that at certain combinations of temperature and strain rate, the strength of MMCs deteriorates (*e.g.*, A1 1-40) and true stress values are comparable to that of the unreinforced alloy. A critical strain rate has been identified, by proposing a model, below which A1 1-40 loses its strength. This has been verified using experimental data.

Unlike fiber-reinforced MMCs[2], no transition in mechanical behaviour has been observed in particle-reinforced MMCs. The existing model[4] has been modified to explain this phenomenon in terms of rate of dislocation accumulation and annihilation at the particle–matrix interface. The calculations show that the rate of climb of dislocations at the particle–matrix interface is much

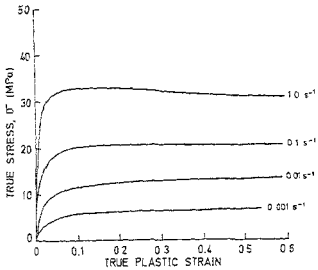

FIG. 1. True stress *versus* true strain curves for Al 8-40 at 550 C at different strain rates.

faster than that at fiber–matrix interface and consequently there is no stress build up in the particle. This supports the absence of transition in mechanical behaviour in particle-reinforced MMCs.

The kinetic analysis of hot deformation of MMCs using a rate equation shows that the stress exponent values are much higher than that of the unreinforced alloy. Similarly, the apparent activation energy values for hot deformation of MMCs are at least two times greater than the activation energy for self-diffusion in Al.

The processing and instability maps (Figs 2, 3) have been developed for all the MMCs and also for the unreinforced alloy. It has been found that the DRX is the dominant softening mechanism responsible for improved hot ductility (reduction of area) and efficiency of power dissipation. Moreover, microstructural observations confirm the occurrence of DRX in certain combina-

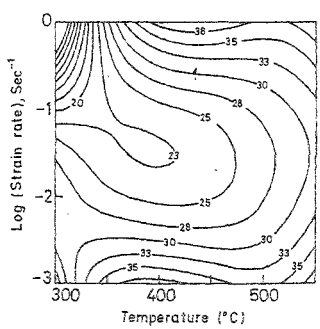

FIG. 2. Power dissipation map for Al 1-20 at a strain of 0.5.

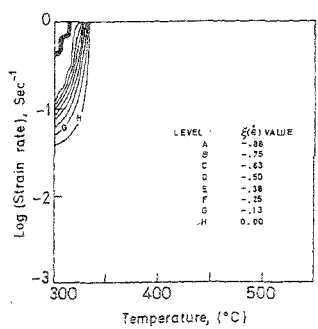

FIG. 3. Instability map for Al 1-20 at a strain of 0.3.

tions of temperature and strain rate. The strain rates at which DRX occurs was determined by the interaction of dislocations/subgrains and particles (Mg_2Si, intermetallic, etc.) at their respective temperatures. Particle-stimulated nucleation is thought to be the mechanism for DRX in MMCs. To find out the rate-controlling process a model has been proposed to determine the rate of nucleation in MMCs. Nucleation and growth rate[6] calculations prove that DRX in MMCs is a growth-controlled process. The domain of macrocrack formation has also been identified in Al 8-40 which is associated with high efficiency of power dissipation.

Microstructural instabilities have been observed at relatively lower temperatures and higher strain rates. These are manifested as localized plastic deformations around the particles and excessive deformation of grains in MMCs and the unreinforced alloy, respectively.

4. Conclusions

In SiC_p-reinforced Al 6061 alloy matrix composites the true stress values are a strong function of both temperature and imposed strain rate. However, the true stress values are found to be a weak function of microstructural parameters, such as size and volume fraction of SiC particles. This is attributed to the occurrence of diffusional relaxation in MMCs. Analysis of the data shows that there is no transition in mechanical behaviour in particle-reinforced MMCs, unlike fiber-reinforced MMCs. This is due to faster rate of climb of dislocations at the particle–matrix interface compared to fiber–matrix interface. Apparent activation energy values (Q) for the hot deformation of composite materials are found to be higher than that of self-diffusion in aluminium. In SiC_p- reinforced Al 6061 alloy matrix composites the rate of nucleation of dynamically recrystallized grains is a function of particle size, volume fraction of particles and imposed strain rate. Thus, DRX is found to be a growth-controlled process in MMCs.

References

1. ROSLER, J., BAO, G. AND EVANS, A. G. — The effect of diffusional relaxation on the creep strength of composites, *Acta Metall.*, 1991, **39**, 2733–2738.
2. STANFORD-BEALE, C. A. AND CLYNE, T. W. — Extrusion and high temperature deformation of fiber-reinforced aluminium, *Composite Sci. Technol.*, 1989, **35**, 121–157.
3. ASHBY, M. F. — The deformation of plastically non-homogeneous materials, *Phil Mag.*, 1970, **29**, 399–424.
4. HUMPHREYS, F. J. AND KALU, P. N. — Dislocation–particle interactions during high temperature deformation of two-phase aluminium alloys, *Acta Metall.*, 1987, **35**, 2815–2829.
5. PRASAD, Y. V. R. K. — Recent advances in the science of mechanical processing, *Indian J. Technol.*, 1990, **28**, 435–451.
6. DERBY, B. AND ASHBY, M. F. — On dynamic recrystallization, *Scr. Metall.*, 1987, **21**, 879–884.

Thesis Abstract (M.Sc. (Engng))

Early stage plate growth in Cu–Zn alloys—An attempt at the resolution of the bainite controversy by N. Ravishankar

Research supervisor: K. Chattopadhyay

Department: Metallurgy

1. Introduction

There exists a controversy in literature on the mechanism of formation of α_1 plates from β matrix in Cu–Zn alloys. This transformation is believed to be diffusional by some[1,2] while others find it of shear type transformation[3]. Although it is generally agreed that the later stage of growth of α_1 plates involves diffusion[4–6], the scenario during the early stage has not been resolved completely. Reports of composition analysis have been inconsistent[1,7] and therefore no definite conclusion could be drawn from them. The question of inheritance of long-range order has also not been established conclusively. This prompted a study of the morphology and crystallography of growing α_1 plates[2]. The main conclusions drawn from the above work are as follows:

(a) at an early stage, a coherent, fault-free α_1 plate is obtained,

(b) α_1 plates formed from the ordered matrix have a disordered structure, and

(c) the later stage of growth involving the thickening of the α_1 plates occurs by a ledge-controlled mechanism.

The validity of (a) is questioned due to the lack of evidence of diffraction in the early stage plates,[8,9] while a recent study[6] claims the presence of superlattice spots indicating that the plate is ordered, thereby, casting doubt on the conclusion (b). The main aim of this work is to take a fresh look at the problem in the light of the above-mentioned inconsistencies. The transformation of α_1 plates to equilibrium α is also considered.

2. Experimental

A Cu-38at% Zn alloy was chosen for the present work. At temperatures around 875°C, it lies in the single-phase β field which has a disordered *bcc* structure. Below 454°C, the *bcc* phase undergoes ordering to form the B2 structure. The high-temperature phase can be metastably retained in the B2 structure by quenching to room temperature. Isothermal ageing of this metastable β between 150 and 350°C yields the α_1 product.

The actual experimental methods adopted are as follows: Thin rectangular strips of the alloy were held in the single-phase β region at 875°C for 3 min and subsequently quenched in saturated brine at room temperature. These samples were then aged at 150 and 250°C for different times in a salt/oil bath. Characterisation of the samples was done mainly using a JEOL 2000 FX-II transmission electron microscope. Twin jet technique was adopted for the preparation of the TEM specimens.

3. Results

The main results of the present study can be summarised as follows:

The small plates during the early stages were found to be coherent with the matrix. The structure of the plates was found to be the same as that of the larger plates by using the microdiffraction technique. Figure 1a shows the microdiffraction pattern corresponding to [0 1 0] zone of the plate shown in Fig. 1b. Since the contrast from these plates is the same as that from the defects in the matrix (dislocations), the microdiffraction technique used thus confirms that these are actually plates and not dislocations. Almost all the contrast features that are expected from a coherent plate have been observed in the present case. The microdiffraction pattern does not reveal the presence of superlattice spots indicating the disordered nature of these plates in the early stages itself. Diffraction patterns from grown plates also do not show any evidence of superlattice

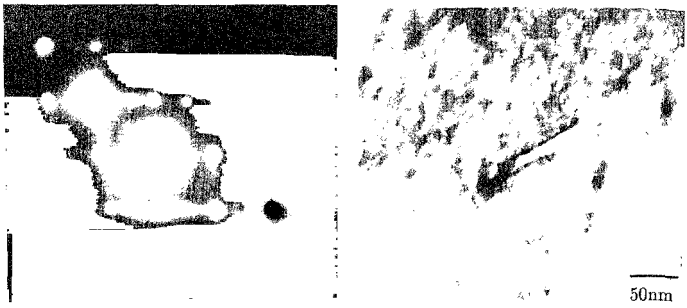

a. b.

FIG. I.a. Microdiffraction pattern corresponding to [0 1 0] zone from an α_1 plate, b. Bright field showing the plate from which pattern is obtained.

spots. It is thus concluded that the plates have a disordered structure. The small, early stage plates do not show any internal structure that is present in the larger plates. On the other hand, surface martensites of similar length scale show the presence of dense faults within.

During the next stage of plate growth, faults develop in the structure. It has been shown that faults are introduced in the plates after a critical size is reached and are often not uniformly distributed.

The last stage corresponds to transformation of the α_1 plates to the equilibrium α phase. It has been shown experimentally that the α phase nucleates within the plates and subsequently grows. It has been assumed by many workers[3] that the transformation takes place in a continuous fashion by the annealing of faults; however, crystallographic analysis reveals that this cannot take place in a continuous fashion but necessarily takes place by nucleation and growth only.

4. Conclusions

The main observations of the present study are as follows:

a) The α_1 plates at very early stages are coherent with the matrix and do not contain faults but martensites of similar length scale contain faults.

b) The plates possess a disordered 9R structure right from the start implying a diffusion-controlled transformation.

c) Faults are formed in the structure only after the strain in the plates exceeds some critical value. The density of faults is not uniform throughout the plate. This is not expected for a transformation by shear.

d) Transformation of α_1 to equilibrium α phase takes place by a nucleation and growth process and cannot come about just by annealing of faults only in the 9R structure.

The above observations suggest the transformation to equilibrium α phase to be diffusion-controlled right from the start up to the final stages.

References

1. LORIMER, G. W., CLIFF, G., AARONSON, H. I. AND KINSMAN, K. R. — Analysis of the composition of α_1 plates precipitated from β' Cu–Zn using analytical electron microscopy, *Scr. Metall.*, 1975, **9**, 271–280.

2. CHATTOPADHYAY, K. AND AARONSON, H. I. — Interfacial structure and crystallographic studies of transformations in β' and β Cu–Zn alloys-I. Isothermal formation of α_1 plates from β', *Acta Metall.*, 1986, **34**, 695–711.

3. CORNELIS, I. AND WAYMAN, C. M. — Phase transformations in metastable β' Cu–Zn alloys-II. Isothermal transformations, *Acta Metall.*, 1974, **22**, 301–311.

4. NAKATA, Y., TADAKI, T. AND SHIMUZU, K. — High resolution analytical electron microscopic study on the bainitic transformation in a Cu–Zn–Al alloy, *Mater. Trans JIM*, 1989, **30**, 107–116.

5. TADAKI, T., UYEDA, T. AND SHIMUZU, K. — High resolution analytical electron microscopic study on the bainitic transformation in a Ag-45% Cd alloy, *Mater Trans. JIM*, 1989, **30**, 117–126.

6. HSU, Y. F., WANG, W. AND WAYMAN, C. M. — Electron microscopy study of the bainitic transformation in a Cu-39.5wt%Zn alloy, *Scr Metall. Mater.*, 1991, **25**, 1059–1064.

7. DOIG, P. AND FLEWITT, P. E. J. — Solute redistribution during the formation of α_1 bainite plates in Cu–Zn and Cu–Zn–Al alloys, *Proc. Int. Conf. on Solid–Solid Phase Transformations*, 1983, TMS-AIME, Warrendale, Pa., pp. 983–992.

8. WU, M. H., PERKINS, J. AND WAYMAN, C. M. — Long range order, antiphase domain structures, and the formation mechanism of α_1 (bainite) plates in a Cu–Zu–Al alloy, *Acta Metall.*, 1989, **37**, 1821–1838.

9. WU, M. H., MUDDLE, B. C. AND WAYMAN, C. M. — Analytical electron microscopy studies of the β_2–α_1 (bainite) transformation in an Ag-45%Cd alloy, *Acta Metall.*, 1988, **36**, 2095–2106.

Thesis Abstract (Ph.D.)

Nonlinear propagation of intense electromagnetic waves in quasar and pulsar plasmas by R. T. Gangadhara

Research supervisors: Som Krishan and Vinod Krishan (Indian Institute of Astrophysics)

Department: Physics

1. Introduction

One of the main problems of astrophysics is the analysis of the radiation of celestial objects in the widest sense of the word. Astrophysical objects such as stars, galaxies, quasars, pulsars can only be studied through the analysis and interpretation of their radiation over the entire electromagnetic spectrum. Some information is also obtained from corpuscular radiation (cosmic rays and neutrinos).

This thesis presents analytical as well as numerical results of radiation–plasma interaction parametric plasma instabilities[1,2] in astrophysical plasmas. These instabilities are shown to play

an important role in (1) generation of nonthermal power-law spectrum[3] of quasars, (2) radio frequency heating[4], (3) polarization variability[5, 6] and (4) rapid flux variability[7] in BL Lacs and quasars and the production of micropulses in pulsars.

2. The role of Compton and Raman scattering in the quasar continuum

The stimulated Raman and Compton scattering can play a significant role in the nonthermal power-law continuum emission of a quasar. There are three ways in which an electromagnetic wave can undergo scattering in a plasma: (i) when the scattering of radiation occurs by a single electron, it is called Compton scattering; (ii) if it occurs by a longitudinal electron plasma mode, it is called stimulated Raman scattering (SRS); and (iii) if it occurs by a highly damped electron plasma mode, it is called stimulated Compton scattering (SCS). The nonthermal continuum of quasars is believed to be produced through the combined action of synchrotron and inverse Compton processes, which are essentially single particle processes. As an example, it is shown that the complete spectrum of 3C 273 can be reproduced[8] by a suitable combination of stimulated Compton scattering and stimulated Raman scattering processes. It is shown that the observed spectral breaks in the blue region could be due to a change in the emission process from stimulated Raman and Compton scatterings. The differential contributions of these stimulated scattering processes for different values of the plasma parameters are also calculated.

3. Anomalous absorption of radiation in astrophysical plasmas

Coherent plasma processes such as parametric decay instabilities (PDI) have been studied[9] in a homogeneous and unmagnetized plasma. These instabilities cause anomalous absorption of intense electromagnetic radiation under specific conditions of energy and momentum conservation and thus cause anomalous heating of the plasma. The maximum plasma temperatures reached are functions of luminosity of the radio radiation and plasma parameters. It is believed that these processes may be taking place in many astrophysical objects. Here, the conditions in the sources 3C 273, 3C 48 and Crab Nebula are shown to be conducive to the excitation of parametric decay instabilities. These processes also contribute towards the absorption of 21-cm radiation.

4. Polarization changes of radiation through stimulated Raman scattering

Stimulated Raman scattering of electromagnetic waves in a plasma medium brings about changes in the polarization[10] of these waves. In this process, an electromagnetic wave undergoes coherent scattering off an electron plasma wave. It is found that some of the observed polarization properties such as the rapid temporal variations, sense reversal, rotation of the plane of polarization and change of nature of polarization in the case of pulsars and quasars, could be accounted for through stimulated Raman scattering.

5. The modulation of radiation in an electron–positron plasma

The modulational instability[11] of a large-amplitude electromagnetic wave propagating in an electron–positron plasma can produce rapid variations in the nonthermal continuum of active galactic nuclei (AGN) as well as in the nonthermal radio radiation from pulsars. The effects such as relativistic mass variation of the plasma particles and the nonresonant, finite frequency electrostatic density perturbations, caused by the large-amplitude radiation field, are taken into account. The radiation from many strong sources such as AGN and pulsars, has been observed to vary over a host of time scales.

We conclude that coherent plasma processes must be included in the study of generation, absorption, polarization and modulation of electromagnetic radiation in high-energy sources such as quasars and pulsars.

References

1. DRAKE, J. F. *et al.* — *Phys Fluids*, 1974, **17**, 778.
2. LIU, C. S. AND KAW, P. K. — *Advances in plasma physics* (Simon, A. and Thompson, B., eds), Vol. 6, p. 83, 1976.
3. WIITA, P. J. — *Phys. Rep.*, 1985, **123**, 117.
4. DAVIDSON, K. AND NETZER, H. — *Rev. Mod. Phys.*, 1979, **51**, 715.
5. COTTON, W. D. *et al.* — *Astrophys. J.*, 1984, **286**, 503.
6. STOCKMAN, H. S. — *Pittsburgh Conf. on BL Lac Objects* (Wolfe, A. M., ed.) 1978, p. 149.
7. HEESCHEN, D. S., KRICHBANM, T., SCHALINSKI, C. J. AND WITZEL, A. — *Astron. J.*, 1987, **94**, 1493.
8. GANGADHARA, R. T. AND KRISHAN, V. — *Mon. Not R. Astr. Soc.*, 1992, **256**, 111.
9. GANGADHARA, R. T. AND KRISHAN, V. — *J Astrophys. Astr.*, 1990, **11**, 515.
10. GANGADHARA, R. T. AND KRISHAN, V. — *Astrophys. J.*, 1993, **415**, 505.
11. GANGADHARA, R. T., KRISHAN V. AND SHUKLA, P. K. — *Mon. Not. R. Astr. Soc.*, 1993, **262**, 151.

Thesis Abstract (Ph. D.)

NMR Study of molecular dynamics and phase transitions in selenates and plumbates of R_2MX_6 family by B. V. Sadashiva Murthy

Research supervisor: J. Ramakrishna

Department: Physics

1. Introduction

Proton spin-lattice relaxation study in a few compounds of the RMX_3, R_2MX_4, R_2MX_6 and $R_3M_2X_9$ family [R = $NH_n(CH_3)_{4-n}$ for $n = 0$ to 4, M = metal atom and X = halogen[1, 2]] have shown interesting features like diffusion and spin-rotation at higher temperatures (> 300 K) and phase transitions in the intermediate temperature range ($77 < T < 300$ K)[3, 4]. At lower temperatures (< 50 K), a few compounds have revealed the presence of tunnelling reorientations[5]. In compounds with symmetric molecules like NH_4, the relaxation is shown to be due to the general reorientation of the NH_4 ion[3, 4]. The symmetry and the dynamics of the NH_4 molecule change with the substitution of the protons by the methyl groups. The C_3 reorientation of the methyl groups as well as the symmetry-restricted motion of the parent ion will then be the effective cause of the spin-lattice relaxation. The activation energies for these motions are found to change with the metal atom (M) and with the halogen (X)[6–10]. A systematic study of the nature and type of molecular motions, with methyl/polymethyl substitution, is expected to yield useful information on the structure and dynamics of molecules and their sub-groups in solids. With this motivation,

molecular dynamics is studied in ammonium, alkyl ammonium hexabromo selenates and alkyl ammonium hexachloro plumbates, through the proton spin-lattice relaxation time (T_1) and the results are presented in this work.

2. Experimental techniques

The compounds have been prepared in the laboratory following the procedures available in literature[3,4]. They are characterised by powder X-ray diffraction, IR, elemental analysis, melting temperature and specific gravity.

The samples are cooled from room temperature (300 K) to 110 K using a conventional gas flow cryostat. The lower temperatures from 110 K down to 77 K is achieved using a specially designed low-temperature cryostat and a low-temperature probe assembly. A special probe assembly is used to heat the samples to the higher temperature (> 300 K).

The proton spin-lattice relaxation time (T_1) is measured from 400 to 77 K at 10 MHz Larmor frequency using the home-made pulsed NMR spectrometer. The second moment (M_2), at various temperatures of study, is computed from the absorption spectra obtained by the Fourier transformation of the FIDs. The results are analysed using appropriate models.

2.1. *Proton relaxation studies in selenates*

Ammonium hexabromo selenate shows six different phases in the temperature range studied (400 to 77 K). Spin rotation and hysteresis are the special features observed in the high-temperature phases (> 300 K) while the general reorientation of the ammonium ion is found to be the cause of relaxation in the low-temperature phases (> 300 K). Methyl ammonium hexabromo selenate shows pronounced phase transitions. Three different types of molecular motions have been identified to cause the spin-lattice relaxation in this compound. The relaxation is due to the correlated motion of CH_3 and NH_3 groups at higher temperatures. The dynamics changes over to uncorrelated motion of NH_3 and CH_3 groups at lower temperatures (< 150 K). Significant effect of the torsional motion of the methyl ammonium ion is seen in the intermediate temperature range (200–155 K), where the observed relaxation time is shortened. Dimethyl ammonium hexabromo selenate shows diffusion in the high-temperature region (> 370 K) followed by spin rotation and the flip motion of the dimethyl ammonium ion (370–222 K). An unusually small T_1 minimum is observed around 171 K. It is attributed to DMA reorientation and the torsion of the dimethyl ammonium ion. In the low-temperature range (< 150 K) the relaxation is caused by the C_3 reorientation of unequivalent methyl groups. Trimethyl ammonium hexabromo selenate has not shown any phase transitions in the temperature range (387–77 K) studied. The relaxation behaviour reveals the presence of unequivalent trimethyl ammonium ions and unequivalent methyl groups in this compound. The presence of unequivalent ions is also observed in tetramethyl ammonium hexabromo selenate. The phase transition observed around 150 K is attributed to the change of motional mode of the tetramethyl ammonium ion from tumbling to torsion.

2.2. *Proton relaxation studies in plumbates*

Methyl ammonium hexachloro plumbate shows dynamics which are similar to those observed in the selenate analogue. However, in the low temperature range (< 150 K) the relaxation is observed to be due to the uncorrelated motion of NH_3 and CH_3 groups followed by the torsional oscillations of the methyl groups. Dimethyl ammonium hexachloro plumbate shows a number of phase transitions, in the range 400 to 77 K. The analysis shows similar dynamics in both the dimethyl ammonium compounds of selenate and plumbate. Trimethyl ammonium hexachloro plum-

bate also shows the presence of unequivalent trimethyl ammonium ions and unequivalent methly groups whose correlation times are closer to each other. Tetramethyl ammonium hexachloro plumbate shows a deep minimum in the high-temperature region and a shallow minimum in the low-temperature region. The high temperature minimum is explained in terms of unequivalent TMS ions and methyl reorientation while the shallow minimum in the low-temperature range is ascribed to methyl reorientation and the torsional oscillations of the methyl groups.

The low activation energies observed in all the above compounds indicate high mobility of the cations of these compounds. The presence of motion even at 77 K, indicated by the reduced second moment, and the T_1 behaviour shows that the relaxation study at temperatures below 77 K might yield interesting features like tunnelling reorientation in these compounds.

References

1. GUTOWSKY, H. S. *et al.* — *Phys. Rev. Lett.*, 1961, **6**, 49.
2. HUBBARD, P. S. — *Phys. Rev.*, 1963, **131**, 1155.
3. NIEMELA, L. K. E. AND OKSMAN, P. H. — *Chem. Phys. Lett.*, 1976, **41**, 174.
4. SVARE, I. *et al.* — *J. Phys. C: Solid St. Phys.*, 1978, **11**, 997.
5. WATTON, A., KOSTER, E., SANDHU, H. S. AND PETCH, H. E. — *J. Chem. Phys.*, 1979, **70**, 5197.
6. IKEDA, R., KUME, Y., NAKAMURA, D., FURUKAWA, Y. AND KIRIYAMA, H. — *J. Magn. Resonance*, 1976, **24**, 9.
7. ISHIDA, H., IKEDA, R. AND NAKAMURA, D. — *Bull. Chem Soc. Jap.*, 1982, **55**, 3116.
8. ISHIDA, H., IKEDA, R. AND NAKAMURA, D. — *Ber. Bunsenges. Phys. Chem.*, 1984, **88**, 546.
9. IKEDA, R., KADEL, R., WEISS, A., ISHIDA, N. AND NAKAMURA, D. — *Ber. Bunsenges. Phys. Chem.*, 1982, **86**, 685.
10. NAKAMURA, D., ITO, K. AND KUBO, M. — *Inorg. Chem.*, 1963, **2**, 61.

Thesis Abstract (Ph. D)

New clock synchronization techniques for digital telecommunication networks by G. M. Rather

Research supervisor: B. S. Sonde

Department: Electrical Communication Engineering

1. Digital telecommunication networks

Ever since the early part of this century, telecommunication has played an increasingly important and crucial role all over the world. Great advances witnessed in business, administration, industry and other economic activities in recent years have been largely through the penetration of telecommunication in everyday life. As a result, telecommunication equipment and systems have received considerable attention with emphasis on design, technology and applications. The ever-growing demand for telecommunication services of various types has made it necessary to move away from the earlier analog approach to the modern digital technique in the post-'60s period, being greatly influenced by the rapid progress in semiconductor and microelectronics technologies in this period. Thus, modern telecommunication terminal equipment, transmission and

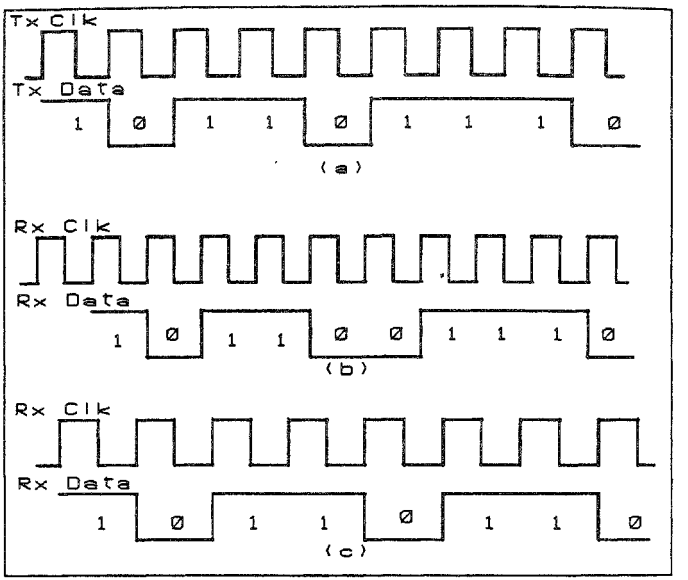

FIG. 1. Slip in digital telecommunication. (a) Transmitter CLK and digital signal waveforms. (b) Condition: Rx. Clk > Tx. CLK; Result: Duplication of Bit B_5; (c) Condition: Rx. Clk < Tx. CLK; Result: Loss of bit B_6.

switching systems, etc., are now based on digital electronics. Also, voice-based services have been considerably supplemented by other nonvoice information services like text, facsimile, image and data. This has resulted in the evolution of integrated services digital network (ISDN) as an extension of conventional telecommunication and the data rates/services provided are now continuously increasing. Recent developments in satellite communication, fibre optics, etc., have now made the digital telecommunication network an important national and international resource all over the world. Hence, digital telecommunication is being studied and investigated regularly to improve its performance and capabilities.

2. Network clock synchronization

Telecommunication network resources like user-interface equipment, transmission links and switching centres(nodes), etc., are necessary for establishing end-to-end connectivity. The synchronization of terminal equipment and the network nodes is an essential requirement for efficient functioning of the digital telecommunication network. This requires that all the nodes of the network operate at the same clock frequency. This can facilitate the correct recovery of each bit in the transmitted digital bit stream at the receiver end which is important for the correct recovery of the embedded information in the digital signal received. The received data can contain errors

due to a number of impairments, which result in a reduced network performance. One of the major impairments in digital telecommunication is the mismatch in the transmitted bit rate and the recovered bit rate at the receiving end. These rates are decided by the clock sources present in both the transmitter and the receiver. The clock source at the transmitter end decides the transmission rate of the digital signal and the receiver clock decides the recovered rate of the same digital signal. A mismatch in the frequencies of these clock sources can result in a loss of some of the information bits or a duplication. This effect shown in Fig. 1 is commonly known as slip[1–4]. The slip rate (number of slips per unit time) decides the performance of the digital telecommunication network[5]; and therefore, it is necessary that this rate should be ideally zero for perfect network clock synchronization.

2.1. *Practical network clock synchronization*

In practical systems, the slip rate is finite. This calls for the use of appropriate network clock synchronization techniques in digital telecommunication networks to minimize the slip rate. One scheme for this purpose is synchronizing the clock sources of the transmitter and the receiver, as shown in Fig. 2. However, in a large distributed network such as PSTN, where each node in the network has its own clock source, synchronizing the various clock sources together is a challenging task of great importance to the network operation. Important issues which arise in a large distributed network during clock synchronization are[6]:

* Active communication taking place among many nodes at any given time;
* Significant internodal delays in the system, being dependent on environmental factors;
* Performance dependence of all the services on the switching office clock due to the shared nature of the switching office resources;
* Service-dependent nature of tolerance to slip; *e.g.*, voice services having superior tolerance as compared to image, data and text services.
* Need for effective distribution of clock synchronization information in the network;
* Interdependence of separately administered interconnected networks; whose number, variety and size are expanding day by day.

These issues make it necessary to incorporate suitable clock synchronization techniques in all large distributed digital telecommunication networks so as to improve the system efficiency, performance and reliability.

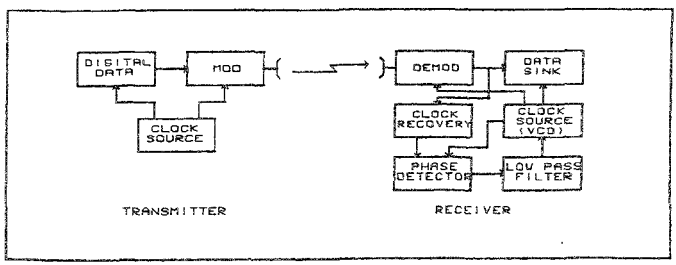

FIG. 2. Receiver clock synchronization: Block schematic.

2.2. *Current approaches*

In the last few decades, different techniques have been proposed, tested and adopted for synchronizing the clock sources of large networks like PSTN, to effectively address the above issues. Important ones are[7,8]:

a) *Plesiochronous technique*: Here, each network node is equipped with a highly robust clock source, preferably an atomic clock. International telecommunication is generally supported by plesiochronous links.

b) *Master slave(MS) technique*: Here, all the clock sources within the network are made to operate at the same frequency and phase, by synchronizing them to a single highly stable clock source which may be internal or external to the network. Hierarchical MS (HMS) technique with self-organizing features has been adopted in most parts of the world for synchronizing national PSTNs.

c) *Mutual clock synchronization(MCS) technique:* Here, all the clock sources in the network, mutually control each other by allowing them to share the clock information among themselves and arrive at a common network timing and frequency. The technique is presently in operation in UK telecom network along with HMS technique. Also, Royal Airforce of Netherlands uses this technique for synchronizing its communication network.

An indepth study of the current approaches to network clock synchronization has brought out its merits and demerits (Table I).

2.3. *Need for a new approach*

Looking at current developments in digital telecommunication networks and the emerging trends in this area, it is preferable that network clock synchronization techniques meet the following additional requirements:

(i) Facilitate rapid expansion of digital telecommunication networks easily as and when required to meet the increasing demand for the services.

Table I
Current clock synchronization techniques in PSTN: merits and demerits

Technique	*Merits*	*Demerits*
Plesiochronous	Simple implementation Easy network expansion No synchronization hardware Suitable for large networks	Costly clocks Frequent clock updating required Clock size large; Large power consumption and short life (3-5 years)
Master slave (Hierarchical)	Simple implementation Flexible network expansion Simple synchronization hardware Suitable for large networks	Centralized clock control Back-up master clock required Master and backup clocks costly Clock stability dependent on master only Accumulation of phase errors along the hierarchies
Mutual clock synchronization	Distributed control Robust synchronization Improvement in clock stability Low stability clocks useable Low capital and maintenance costs	Complex synchronization hardware Tedious and costly network expansion Practical for small number of nodes Internodal delay affecting the system clock frequency and phase

(ii) Support increasing bit rates necessary for providing broadband services like video, image and data.
(iii) Provide end-to-end digital connectivity necessary for ISDN.
(iv) Improve overall network performance using adaptive techniques.
(v) Bring down the cost of the telecommunication services.

These requirements make it necessary that any network clock synchronization technique to be used in the future should have facilities for:

* Easy and flexible network expansion;
* Improvement in network clock stability;
* Reduction in accumulation of phase errors;
* Distributed clock control, and
* Compatibility with the existing network topologies.

As seen from Table I, none of the current techniques of network clock synchronization is capable of facilitating all the above requirements individually. Therefore, in order to realize a new network clock synchronization technique as envisaged, a different strategy needs to be employed. In this context, combining the popular network clock synchronization techniques, *viz.*, HMS and MCS has provided a new direction. This approach has resulted in the development of two new clock synchronization techniques, *viz.*, HMCS and WHMCS. These techniques not only support the hierarchical network topology similar to the HMS technique facilitating the easy and flexible expansion of the networks, but also use distributive clock control, an important feature of the MCS technique, to maintain close frequency and timing control in the overall network. This has been verified in the laboratory using analytical and experimental techniques (Tables II and III).

3. Conclusions

Main conclusions drawn from the analytical and experimental studies and observations are now summarized:

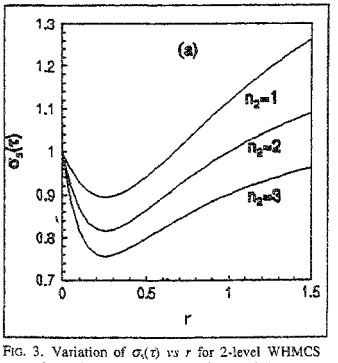

FIG. 3. Variation of $\sigma_1(\tau)$ *vs* r for 2-level WHMCS networks; $\sigma_1(\tau):\sigma_2(\tau)::1:2$ (simulation results).

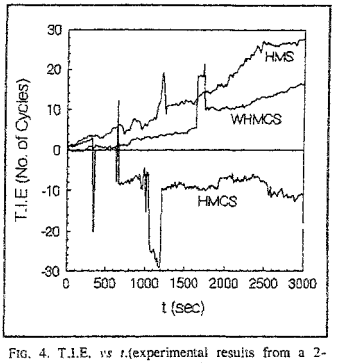

FIG. 4. T.I.E. *vs* t.(experimental results from a 2-node, 2-level hierarchical network of VCXOs).

Table II
HMS, HMCS and WHMCS techniques: Main observations from analytical study

Analytical study	*Parameter*	*HMS*	*HMCS*	*WHMCS*	*Remarks*
Steady state	Steady-state frequency (f_s)	Decided by master clock only.	Decided by all clock sources; Equal to average of all f_{os}s.	Decided by all clock sources; Equal to weighted average of all f_{os}s.	WHMCS most superior
	Clock stability [$\sigma_s(\tau)$]	Decided by master clock only.	All clock sources influence this equally; Maximum, if all clocks are of the same stability.	Decided by all clock sources; Maximum when $r = r_{pot}$.	
Transient state	Frequency	All nodes experience the same frequency shift if master node experiences a frequency step change. No effect, if any other node experiences a frequency shift.	Frequency shift is similar irrespective of the node experiencing the frequency step change. Internodal delay dynamics affect the frequency.	Magnitude of the frequency shift depends on the level of the node experiencing frequency step. Internodal delay dynamics affect the frequency. The effect is less than the HMCS.	WHMCS most superior
	Phase	All the nodes experience a phase error if the master clock experiences a shift. An intermediate node and its subnodes experience a phase error if the intermediate node experiences a frequency step change. Delay dynamics introduces phase errors;	Phase of all the nodes is affected; Magnitude of the phase errors is the least; Internodal delay dynamics affect the phase of different nodes.	Magnitude of phase error is more if a higher level node experiences a frequency step. The effect is less than the HMS case. Internodal delay dynamics affect the phase of different nodes.	
Noise transfer	Phase errors (T.I.E.s) accumulation	Highest of all the techniques. Occurs along the hierarchies.	Lowest of all the techniques; Identical for the highest and the lowest level node (linear network). Output noise minimum if all the ousrces are identical.	Lower than HMS. Output noise is minimum when $r = r_{opt}$.	WHMCS most superior

Table III
HMS, HMCS and WHMCS techniques: Main results from experimental study

Study	*Network*	*Test performed*	*HMCS*	*WHMCS*	*WHMCS*	*Remarks*
Steady state	2 Node, 2 level	$\Delta f = 30 \pm 2$Hz Applied at	Shift in f_s	Shift in f_s	Shift in f_s	In HMS networks, f_s and $\sigma_s(\tau)$ are decided by master node (Level I) only.
		Node 1, level 1	30 Hz	15 Hz	22 Hz	In HMCS networks, all nodes affect f_s and $\sigma_s(\tau)$ equally.
		Node 2, level 2	Nil	14 Hz	10 Hz	
		Network stability ($\sigma_s(\tau)$)	0.208×10^{-7}/2 s 0.391×10^{-7}/10 s 0.919×10^{-7}/20 s 0.926×10^{-7}/100 s	0.153×10^{-7}/2 s 0.261×10^{-7}/10 s 0.389×10^{-7}/20 s 0.604×10^{-7}/100 s		In WHMCS networks, all nodes affect f_s and $\sigma_s(\tau)$; But the higher level nodes having more weightage affect more.
	5 Node, 3 level	$\Delta f = 30 \pm 2$Hz Applied at	Shift in f_s		Shift in f_s	
		Node 1, level 1	30 Hz	No test conducted	12 Hz	
		Node 2, level 2	Nil		8 Hz	
		Node 4, level 3	Nil		5 Hz	
		Network stability ($\sigma_s(\tau)$)	0.304×10^{-7}/2 s 0.843×10^{-7}/10 s 1.199×10^{-7}/20 s	No test conducted	0.227×10^{-7}/2 s 0.604×10^{-7}/10 s 0.677×10^{-7}/20 s	
Transient state		V_c step applied at				
	2 Node, 2 level	Node 1, level 1	Both nodes get affected and system stabilizes at a new f_s decided by level 1 node.	Both VCXO nodes are affected. The system operation stabilizes at new f_s which is average of the two f_{co}s.	Both nodes are affected, But, shift in f_s is more.	In HMS networks, (i) all nodes experience frequency and phase change if master node experiences a transient; (ii) If transient appears at a node other than the master node, only phase error with respect to master node is introduced in the node and its subnodes;
		Node 2, level 2	Node 2 only affected temporarily	Both VCXO nodes are affected The system operation stabilizes at new f_s which is average of the two free f_{co}s.	Both nodes are affected, But, shift in f_s is less.	In HMCS networks, all nodes experience a frequency and phase change irrespective of the node and its level which experiences a transient.
	5 Node, 3 level	Node 1, level 1 Node 2, level 2 Node 4, level 3	All nodes are affected. Nodes 2, 4, and 5 affected temporarily. Node 4 affected temporarily.	No test conducted	All nodes are affected; But, shift in f_s is more. All nodes are affected; But shift in f_s is less.	In WHMCS networks, all nodes experience a frequency and phase change. But magnitude of effect is more if higher level nodes experience a transient.
Noise transfer (Accumulation of T.I.E.s)		T.I.E. measurement				
	2 Node, 2 Level	Between levels 1 & 2	Accumulation fast	Accumulation slowest	Accumulation moderate.	T.I.E. accumulation is fast and the highest in the HMS networks; Moderate in the WHMCS networks and the least in the HMCS networks.
	5 Node,	Between levels 1 & 3	Accumulation fast	No test conducted	Accumulation less as compared to HMS.	

(i) *Improved network clock stability*: The WHMCS technique offers the best system clock stability amongst all the hierarchical clock synchronization techniques under the condition $r = r_{opt}$, (Fig. 3) where,

$$r_{opt} = \left(\frac{\sigma_{d-1}(\tau)}{\sigma_d(\tau)} \right)^2$$

with $\sigma_{d-1}(\tau)$ and $\sigma_d(\tau)$ being the free running frequency stabilities of the clocks at two successive hierarchical levels of the network. This ensures that the resulting slip rate is minimum.

(ii) *Reduction in the accumulation of TIEs*: Both the HMCS and the WHMCS techniques show a reduction in the accumulation of TIEs along with an increase in hierarchy (Fig. 4). This helps in achieving close timing and frequency control and facilitating increased bit rates to end users, than possible by the conventional HMS technique.

(iii) *Easy and flexible network expansion*: Both the HMCS and the WHMCS techniques support hierarchical network topology similar to the HMS. This helps in easy and flexible network expansion.

(iv) *Adaptive clock synchronization*: The HMCS and the HMS techniques are indeed special cases of the WHMCS technique, obtainable by adjusting the value of $r = 1$ and 0, respectively, in the network. This can facilitate adaptive clock synchronization in any hierarchical network and use of all the three techniques, *viz.*, WHMCS, HMCS and HMS in different parts of a complex network, including ISDN, B-ISDN as may be required.

(v) *Hardware requirements*: The new technique proposed uses conventional LSI/VLSI devices, which can be either of the standard type or based on ASICs of one type or the other, *viz.*, full custom, semi-custom, etc.

References

1. COOPER, C. A. — Synchronization for telecommunications in a switched digital network, *IEEE Trans.*, 1979, **COM-27**, 1028–1033.
2. KARTASCHOFF, P. — Synchronization in digital communication networks, *Proc. IEEE*, 1991, **79**, 1019–1028.
3. LUETCHFORD, J. C. *et al.* — Synchronization of digital networks, *IEEE Trans.*, 1980, **COM-28**, 1285–1290.
4. — CCITT recommendations G.701, Vocabulary of digital transmission and multiplexing, and pulse code modulation (PCM) terms, Red book, 1984.
5. — CCITT recommendation G. 822, Controlled slip rate objectives on an international digital connection, Geneva, 1980 (further amended).
6. ABATE, J. E. *et al.* — AT&T approach to the synchronization of telecommunication networks, *IEEE Commun. Mag.*, 1989, 35–45.
7. LINDSEY, W. C. *et al.* — Network synchronization, *Proc. IEEE.*, 1985, **73**, 1445–1468.
8. PAN, J. W. — Synchronizing and multiplexing in a digital communication network, *Proc. IEEE*, 1972, **60**, 594–601.

Thesis Abstract (Ph. D.)

Intelligent decision support systems for project planning and scheduling by Sunil J. Noronha

Research supervisor: V. V. S. Sarma

Department: Computer Science and Automation

1. Introduction

Intelligent decision support systems (IDSS) are computer programs that employ expert system tools and techniques and a large amount of domain knowledge to interactively assist a user in structuring and solving decision problems. They are the product of a synthesis of methods from two fascinating disciplines: artificial intelligence and decision analysis. This study explores the

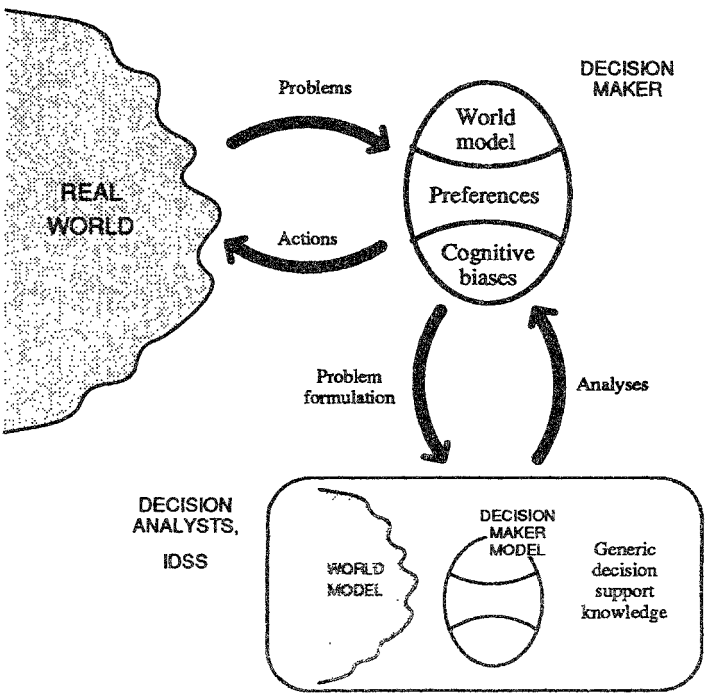

FIG. 1. A systems view of decision making.

confluence of these two disciplines, from a pragmatic engineering viewpoint, with the objective of designing an intelligent decision support system for a real-world task, project management. Figure 1 displays the context of the problem.

2. Planning and scheduling

This study illustrates the issues of IDSS design in the context of project management. Project management is a real-world problem that provides adequate richness in exploring decision tool design at varying levels of complexity, and for developing techniques with a wide range of applicability. It contains elements of, and relates to, many important problems facing both, operations managers and AI researchers: job scheduling and resource allocation, task planning, management of risk or uncertainty, etc. We survey planning and scheduling problems, develop a taxonomy of these problems, and position project management tasks with regard to this taxonomy[1]. The benign–hostile worlds spectrum of task complexity is developed with the classic blocks world planning example of AI, and was used to formulate several versions of the project scheduling class of problems.

3. Knowledge representation

The power of an IDSS is derived from the high-level domain knowledge that it contains, which can be of many types and can be derived from multiple knowledge sources. It includes knowledge of project objects and their properties; statements about the world and relationships between them; knowledge of uncertainties involved in these statements, *e.g.*, probabilistic or fuzzy; the goals and the preference system of the decision maker; constraints on the problem; evolution of the state of the project over time; problem-solving methods; etc. Capturing this knowledge in all its variety requires powerful knowledge structures for its implementation, and thus a taxonomy is developed with the objective of matching appropriate knowledge structures to each knowledge type. Use of qualitative reasoning, fuzzy sets, and a formalism for combining multiple uncertainty handling mechanisms are explored.

Two knowledge structures receiving special attention in this study are the Petri net and the project influence graph (PIG). Petri nets are well suited to the representation of any dynamical system, and therefore capture valuable information relating to the progress of the project. The thesis describes project modeling with Petri nets and the implementation of a Petri net simulator using object-oriented programming in CLOS. Project activities are modeled with an immediate-transition–place–timed-transition combination, and the marking of the Petri net is used to depict the state and progress of the project. The language of Petri nets permits a number of project conditions to be modeled, *e.g.*, contention for resources, start and finish time constraints, etc. demonstrating the use of generalized stochastic Petri nets to handle uncertain activity durations, and collect statistics such as probability of missing a deadline with a general-purpose Petri net simulator.

4. Project influence graphs

Classical project management tools such as the PERT chart were not designed for decision support; they were designed for the second phase of project management, namely, project scheduling. They do not document why the activities in the graph have been selected from among various alternatives, and how their durations and resource allocations have been estimated; nor do they document other nonscheduling decisions that have been taken in the first phase of project management, namely, project planning. The thesis introduces project influence graphs (PIGs) as a

powerful new tool for decision support, by combining ideas from influence diagrams[2], AND-OR graphs[3], and conceptual graphs[4]. Because of the influence diagrams' rigorous underpinning of probability theory, PIGs are used to propagate the effects of new information and changing assumptions on the decision maker's beliefs to support inferencing and prediction. Modeling of project decision problems with PIGs is illustrated with several examples, and the ability to reason both qualitatively and numerically with PIGs is brought out.

Project influence graphs have the following advantages:

- PIGs are highly expressive.
- They support goal decomposition and hierarchical abstraction.
- PIGs support qualitative reasoning.
- They serve as a natural decision documentation tool.
- They have a focusing effect and help in the visual analysis of a problem.
- PIGs are an excellent communication tool between people.

In other words, PIGs provide a high-level user-friendly front end to an IDSS for decision analysis.

5. Scheduling

During the second stage of project management, project scheduling, the IDSS provides intelligent scheduling support through AI-based heuristic search techniques. The classical resource-constrained project scheduling problem is formulated as state space search, and a simple but effective heuristic evaluation function is used with the A* algorithm to obtain optimal solutions for small problem instances. The same algorithm placed in the generalized branch-and-bound framework is used with pruning to solve larger problems for approximate solutions.

In order to smoothly integrate all these techniques, a complete top-level design of an IDSS is proposed in the thesis. Some of the architectural issues addressed include modularity of design, explanatory capabilities and focus of control.

References

1. NORONHA, S. J. AND SARMA, V. V. S. — Knowledge based approaches for scheduling problems: A survey, *IEEE Trans.*, 1991, **KDE-3**, 160–171.
2. HOWARD, R. A. — Knowledge maps, *Mgmt Sci.*, 1989, **35**, 903–922.
3. KANAL, L. N. — Problem solving models and search strategies for pattern recognition, *IEEE Trans.*, 1979, **PAMI-1**, 193–201.
4. SOWA, J. F. — *Conceptual structures. Information processing in minds and machines*, 1984, Addison-Wesley.

Thesis Abstract (Ph. D.)

Studies on pollution performance of metal-oxide surge arresters by R. S. Shivakumara Aradhya

Research supervisors: B. I. Gururaj and M. Ramamoorty (CPRI)

Department: High Voltage Engineering

1. Introduction

Surge arresters play a pivotal role in coordination of insulation in EHV substations. Over the years, metal-oxide arresters (MOAs) are increasingly being used because of their enhanced capabilities for energy handling, temporary overvoltages as well as simplicity in construction. Most aspects of design and selection of MOAs are well understood and national and international standards[1] for them have been published. However, certain aspects are still under active investigation. One of them is their pollution performance which, indeed, presents a confusing picture. When the MOAs were newly introduced, some of them performed well even in heavy pollution zones while others failed under low pollution and, sometimes, even under light drizzle. Therefore much attention has been given to this problem in most countries.

The effects of wet pollution on the MOA are to reduce the external insulation strength, cause internal discharges and heating of the internal elements. As the station insulation design with regard to pollution is standardized and methods to prevent effects of partial discharges by special coatings on the MOA elements are adopted by most manufacturers, failures due to these causes are less in modern MOAs.

A survey of available literature showed that thermal performance of MOAs under polluted conditions is the only aspect under active debate in various fora. Many attempts are being made to investigate this behaviour through monitoring of arresters in the field, mathematical models and by adopting test methods already standardized for station insulators and gap-type arresters or modifications of them. More recently, attempts are being made in some European countries to correlate the external charge measurements in the arrester with temperature rise and also to represent site severity using current integrals obtained in natural pollution test sites. The adequacy of a pre-heat temperature of 60°C already adopted in the standards, in view of possible higher temperatures due to pollution effect, is also being investigated. Many methods[2]—uniform wet contamination (slurry coating), nonuniform wet contamination method (ANSI method and others) and salt-fog method—have been proposed.

2. Mathematical model of polluted arresters

It is difficult to perform and compare these test results on various types of arresters on a uniform basis. Hence, mathematical modelling emerges as a tool of great versatality for such comparisons. The MOA model suitable for pollution study has two parts, electrical and thermal models. The electrical model[3] comprises the V-I characteristics of the MO element, the pollution conductance variation representing wetting and drying processes, the capacitive coupling between the element column and the pollution layer, and stray capacitances like the housing-to-ground, grading ring-to-element and flange-to-element capacitances. The thermal model[4] represents the thermal capacities of the various components of the MOA, heat transfer from elements to the housing and metallic flange, and heat transfer from the housing to the ambient atmosphere. The computed power loss in the MO elements during the pollution activity on the housing is input to the electrical analog of the thermal circuit for computing temperatures attained by the elements and the porcelain housing along the height of the arrester. In the first part, integrated mathematical models of electrical and thermal circuits of single and 2-unit polluted MOAs have been developed. These models have been validated by test results. Sensitivity of parameters like capacitance between the MOA element column and the pollution layer, its initial conductance and its drying time have been established for the first time. Simulation of test methods to correlate the element temperature rise and the external current integrals have been successfully performed. Difficulties in simulating salt-fog test have been discussed.

3. Tests on MOAs

The second part deals with tests on arresters—single and multiunit using various test procedures. The need for pollution testing of single unit arrester as per ANSI method can be questioned as simulation and the laboratory tests on them yielded very low temperature rise. Tests on 2-unit MOAs were performed to establish the merits and limitations of the procedures and to examine the possibility of site severity representation by the current integral method in these tests. From the element temperatures recorded during the tests, it could be concluded that they are proportional to the external charge on the arrester. Uniform wet contamination and salt-fog tests result in higher temperatures compared to the nonuniform wet contamination (ANSI) test. All these tests resulted in varying spread in the measured maximum temperatures. The results obtained also indicate that the test methods forcing nonuniform voltage distribution (ANSI test) result in less spread for the highest temperature attained by the elements. The cause for spread of results is explained by the initial conductance of the slurry and its variation with ambient humidity conditions. This aspect is not covered in the available literature.

4. Site severity simulation in tests on MOAs

In the third part, the possibility of simulation of site severity conditions has been examined in some detail. Comparing the uniform and nonuniform wet contamination (ANSI and other methods) as well as the salt-fog method, it emerges that only uniform wet contamination and salt-fog tests can be representative of industrial and marine pollution, respectively. Problems and prospects in the implementation of the most recent IEC proposal have also been briefly discussed.

References

1. Metal oxide surge arresters without gaps for ac systems, *IEC Standard* 99-4, 1991.
2. BARGEGIA, DE NIGRIS, M., PIGINI, A. AND SIRONI, A. Comparison of different test methods to assess the thermal stresses of metal-oxide surge arresters under polluted conditions, *IEEE Winter Meeting*, 1992, paper no 92 wm 231-PWRD.
3. HINRISCHSEN, V. AND PEISER, R. Simulation of the electrical and thermal behaviour of metal oxide surge arresters under ac stresses, paper No. 26-04, IS 1989.
4. LAT, M. V. Thermal properties of metal-oxide surge arresters, *IEEE Trans.*, 1983, **PAS-102**, 2194–2202.

Thesis Abstract (Ph. D.)

Studies on the voltage-current characteristics of duct type electrostatic precipitator under dc/pulse energizations by B. S. Rajanikanth

Research supervisor: B. R. Prabhakar

Department: High Voltage Engineering

1. Introduction

Among the gas cleaning equipment, electrostatic precipitator (ESP) is unique in that it emp electrical forces to separate the particles from the gas stream. An ESP usually consists of a v held at a high potential and a cylinder or a pair of parallel plates, maintained at ground poten

The wires are called as discharge or corona electrodes and the grounded plates are known as collectors. Further, a wire–cylinder geometry is known as a pipe-type ESP and a wire–plate geometry is called as a duct-type ESP. An increase in the voltage enhances the corona process near the wires resulting in an increase in current density in the inter-electrode region. This results in an enhanced particle charging and collection. Thus the charging and collection processes are mainly governed by voltage–current (V–I) characteristics.

The V–I characteristics in dust-free conditions have been considered as reference for those obtained under operating conditions[1]. The characteristics help in diagnosing the electrical problems associated with ESP operations. The V–I characteristics are mainly governed by the design of the corona electrodes and mode of energizations. Previous research work indicates the importance of the helical wire and barbed plates as corona electrodes[2,3]. The research work also indicates the importance of sub-microsecond pulse energizations[4] in preventing back corona, a problem associated with conventional dc energizations when tackling high-resistivity ducts. A mathematical model of V–I characteristics will enable a detailed analysis of the current and voltage under the operating conditions prior to the design of an ESP. However, not much work has been reported in the literature about the experimental and theoretical investigations of dc/pulse charging of helical wires and barbed plate ESPs. The present research work reports the experimental studies conducted in clean air on a section of a duct-type ESP, as this is the one which is commercially used. The experiments were conducted both with dc and pulse energizations with helical and barbed plate as corona electrodes. Mathematical models have been proposed for the first time to predict dc and pulse V–I characteristics of duct-type ESPs.

2. Experimental setup

Experiments have been conducted on one section of a pilot plant duct-type ESP. The ESP consists of 2 collector plates of 200 cm height and 50 cm width. The helical wires used are of 183 cm in length and 2.7 mm in diameter. The wire–wire spacing was varied from 4.5 to 15 cm. The other type of corona electrode, barbed plate, consists of about 555 cylindrical pins fixed to a plate of length 183 cm and width 30 cm. Two barb diameters were used in the studies. The barb lengths studied were 13, 18 and 23 mm. The vertical barb–barb spacing was maintained at 25.4 mm. The duct spacing was varied from 100 to 300 mm.

A 250 kV, 25 mA set was used for dc energization and a 250 kV repetitive surge generator, a modification MARX impulse generator, was used for pulse energization. For the combined dc/pulse energization, a high resistance is used on the dc side to block the pulse and a capacitor is used on the pulse side to block dc.

3. Results and discussion

Experiments were conducted first with helical wire ESP at various wire–wire spacings and duct spacings. At higher duct spacings, the rate of rise of current density is very slow at lower voltages and raises very quickly as the breakdown voltage is approached. Studying the effect of wire–wire spacing, appreciable change in dc current is seen particularly at lower wire–wire spacings. The results also highlight the role played by the ratio of wire–wire to wire–plate spacings. The experiments with barbed plate ESP were conducted at various barb–barb lengths, barb diameters and horizontal barb–barb spacings. There exists a critical horizontal barb–barb spacing, for a given duct spacing and barb length, at which good V–I characteristics are obtained. A comparative study of dc V–I characteristics indicates that barbed plate ESP exhibits good V–I characteristics as compared to helical wire ESP, particularly at lower duct spacings. At these current densities, the barbed plate current density differs both in magnitude and trend.

In the combined dc/pulse energization of helical wire ESP, studying the effect of wire–wire spacing, considerable increase in current density is seen at low wire–wire spacing when one goes from dc energization to pulse energization. When the dc bias is set above the corona onset, the current density shows appreciable increase only after the 60% breakdown voltage is reached, below which it remains constant. To check the effectiveness of back corona with sub-microsecond pulse energization, a simulation of back corona was carried out and it was observed that a weak back corona sets in when the dc bias is set above the corona onset.

Prediction of the dc V–I characteristics of the helical wire and barbed plate ESP has been made by proposing a modified approach to the existing dc model of straight wire ESP[5]. The basic technique behind the model lies in numerically solving the Poisson's equation and current continuity equations simultaneously, subject to the existing boundary conditions. Finite-difference method is employed for solving the equations. It has been shown that a helical wire can be represented by a rough straight wire. The choice of the roughness factor depends on the pitch of the helical wire. Similarly, a barbed plate housing multicolumn barbs can be represented by multicolumn wires. The barb length was represented by an effective roughness factor of the wire. The proposed model is helpful in studying the effect of wire–wire spacing, wire diameter, barb diameter, barb length and barb–barb spacing, on the V–I characteristics. The model is validated against the present experimental results.

The most important contribution of the present research work is the development of a mathematical model to predict the pulse V–I characteristics of a helical wire duct-type ESP. The proposed model begins with the calculation of charge density near the wire using the method suggested by Menegozzi and Feldman[6]. The model then proceeds with the spatio-temporal drift of the space charges, simulating the existing dc model. The 2-dimensional model is developed for a practical case where the dc bias is at or below the corona onset. Though the model is developed for pulse widths of the order of 0.7 μs, it can be applied even for pulse widths of the order of 1.5–2 μs. The predicted results agree well with the experimental results.

4. Conclusions

Experimental studies on duct-type ESP with helical corona wires provide valuable data on the effect of duct spacing, wire–wire spacing and dc bias on the corona current density. This is especially important particularly in wide duct spacings, which are coming into prominence in recent years. Simulation studies on back corona in the presence of high resistivity layers indicate that the sub-microsecond pulses are not very effective in preventing back corona at high resistivities of the order of 10^{14} Ω-cm. Experiments on barbed plate ESP have thrown light on the effect of barb diameter, barb–barb, spacing, etc., on the corona current, as compared to the helical wire ESP. This has provided new data on barbed plate ESP. New mathematical models have been proposed for the prediction of dc V–I characteristics of duct-type ESP operating either with helical wire or barbed plate corona electrodes. The important contribution lies in the development of a theoretical model for predicting pulse V–I characteristics based on simple townsend mechanisms and on modification of the existing dc model. The predicted results are in close agreement with the experimental results.

References

1. OGLESBY, S. JR AND NICHOLS, G. B. *Electrostatic precipitation*, 1978, Marcel Dekker.

2. SEKAR, S. AND STOMBERG, H. On the prediction of current-voltage characteristics for wire-plate precipitators, *J Electrostatics*, 1981, No. 10, 35–43.

3. McKINNEY, P. J., DAVIDSON, J. H. AND LEONE, D. M. — Current distributions for barbed plate-to-plate coronas, *IEEE Trans*, 1992, **IAS-28**, 1424–1431.

4. MASUDA, S., HOSOKAWA, S., TACHIBANA, N., ANDO, T. AND MATSUMOTO, T. — Fundamental behaviour of direct coupled sub-microsecond pulse energization in electrostatic precipitators, *IEEE Trans.*, 1987, **IAS-23**, 120–126.

5. McDONALD, J. R., SMITH, W. B., SPENCER, H. W. III AND SPARKS, L. E. — A mathematical model for calculating electrical conditions in wire-duct electrostatic precipitator devices, *J Appl Phys*, 1977, **48**, 2231–2243.

6. MENEGOZZI, L. N. AND FELDMAN, P. L. — The physics of pulge energization in electrostatic precipitators, *3rd Symp. Transfer and Utilization of Particulate Control Technology*, Orlando, USA, 1981.

Thesis Abstract (Ph. D.)

Developmental studies of an electromagnetic pulse simulator by M. Joy Thomas

Research supervisor: G. R. Nagabhushana

Department: High Voltage Engineering

1. Introduction

A high-altitude nuclear burst gives rise to essentially three effects—blasts, heat and nuclear radiation[1]. About 0.1% of the total energy of the explosion gets converted to extremely high-energy gama rays which move from the burst symmetrically, primarily in the radial direction[2]. They interact with the air molecules and create high-energy electrons, also known as Compton

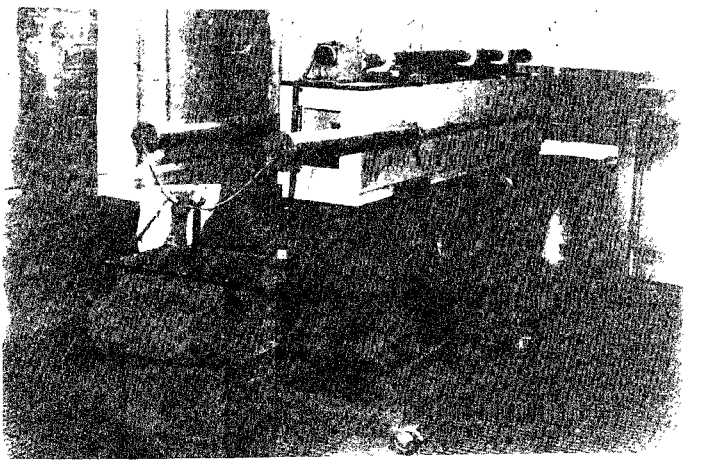

FIG. 1. Transient pulse energy source.

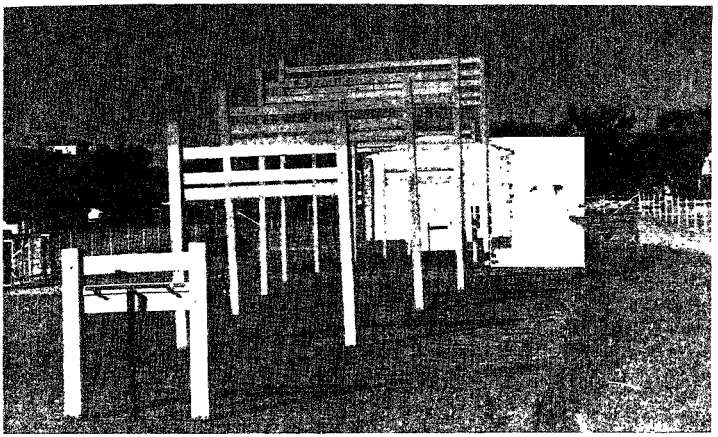

FIG. 2. Illuminator with terminating resistor.

electrons. These Compton electrons are influenced by the Earth's magnetic field and they spiral around the geomagnetic field lines. Asymmetry of these electronic currents results in a resultant electro magnetic pulse (EMP) travelling towards the Earth at the velocity of light[3,4]. Because of the high altitude (>50 km) of the burst this electromagnetic pulse (EMP) covers a very large area over the Earth's surface simultaneously. For example, a high-altitude burst (300 km) of 1MT strength over the geometric centre of India covers the entire Indian subcontinent which includes the whole of India, Pakistan, Sri Lanka and a substantial part of China, Burma, etc.[5] Such an EMP has been estimated to have at the Earth's surface electric fields in the range of 50 kV/m and a transverse magnetic field of 130 A/m. EMP is characterised by a risetime of 10 ns and a duration of 200–500 ns. Such a pulse encompasses a frequency band of a few to 100 MHz[3,6].

The electromagnetic fields produced by the EMP can induce large current and voltage transients in electrical and electronic equipment, causing possible temporary malfunction or damage[3].

The equipment/instruments that can get crippled include: (i) electronic telephone exchanges, (ii) powerline carrier systems, (iii) computers and data links, (iv) computer-based controls and instrumentation of all kinds, (v) electronic control systems used in aircrafts, ships, radars, and (vi) defence communication system, etc.

The energy density[2] at the Earth's surface for an 1 mt burst at a height of 100 km above the Earth's surface is estimated to be about 3 J/m^2. Moreover, the increasing sensitivity of modern electronic devices has greatly enhanced their vulnerability to EMP. Thus there is a great necessity for hardening sensitive electronic circuitry to withstand EMP.

In order to validate the hardening techniques adopted for such electronic circuits and systems against EMP, an actual nuclear environment is neither practical nor desirable. Tests in simulated

EMP environment, therefore, are the only practical means of evaluating the system's vulnerability or hardness.

The present work concerns the development of a parallel plate EMP simulator including electric field, magnetic field and voltage-measuring devices.

2. Design and development of the EMP simulator

The EMP simulator consists of (i) a transient pulse energy source including the peaking circuit and the output switch (Fig. 1), (ii) an illuminator with terminating resistors (Fig. 2) and (iii) the requisite controls. Also, the whole system including the energy source, illuminator and the terminating resistor should have a constant surge impedance to avoid reflections from the junctions.

In this work, a four-stage Marx-type generator with two capacitors/stage and rated 150 kV, 0.01 μF forms the transient pulse energy source. In order to achieve a short risetime for the pulse, a peaking circuit consisting of a peaking capacitor and a pressurised output switch has been used. The peaking capacitor consists of two capacitors in series, each of value of 500 pF. The electrodes of the output switch are tapered in shape so as to match the impedance of the gap with that of the illuminator.

Also the influence of the instant of firing the output switch on the risetime of the pulse was studied computationally. It is seen that when the output switch is triggered with some delay after the voltage peak, the risetime remains almost constant whereas when it is fired before the voltage peak, the risetime increases with the pre-trigger time. Also the peak voltage across the load could reach 1.6 times the Marx generator voltage and this magnitude also depends on the delay in triggering the output switch. A scheme for controlling the instant of firing the output switch using a 50 MW Nd : YAG laser beam has also been developed.

Since the residual inductance of the peaking capacitor plays a crucial role in determining the risetime of the output pulse, it was necessary to measure it. As the inductance involved is only

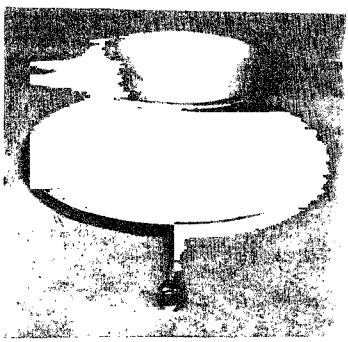

FIG. 3. V-conical sensor.

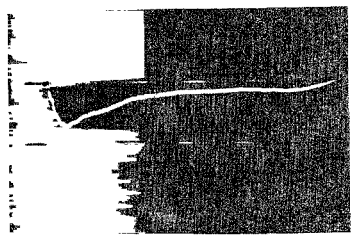

FIG. 4. EMP measured within the working volume. Rise time 10.3 ns, duration 262 ns and peak field 49 kV/m.

about 100 nH, the measurement of the inductance of the peaking capacitor poses considerable difficulty, especially because of its large size due to the high voltage rating (800 kV). After taking considerable care in the measurement, the inductance of the peaking capacitor calculated using the latter portion of the capacitor discharge current oscillogram was 126 nH which is quite reasonable.

For realising the short times to front, the Marx unit has to be compact but the working volume is quite large ($5 \times 5 \times 5$ m). Therefore, the illuminator (the parallel plate structure) has to be tapered on both sides to provide convenient points to connect the transient pulse energy source at one end and the terminating resistors at the other. The tapered portion should also be of constant and appropriate surge impedance. In the present work, the taper angle is 11.4° and the length of the tapered section is 25 m on either side. The top electrode of the illuminator consisted of 21 copper wires and the ground plane consisted of 50×50 mm welded mesh. For the configuration chosen, the illuminator has a surge impedance of 150 Ω and it can support a resonant frequency of 120 MHz.

The parallel plate illuminator structure has also been characterised for its surge impedance using TDR technique and the measured value agrees very well (within the limits of measurement error) with the design value of 150 Ω.

3. Design and development of the sensors

For measuring the transient electromagnetic fields and related quantities like voltage within the working volume of the simulator, broadband sensors and voltage dividers with simple transfer functions are required.

For the measurement of the electric field three different types of sensors, namely, parallel plate dipole (PPD), asymptotic conical dipole (ACD) and V-conical (Fig. 3) sensors were developed. For the measurement of the magnetic field, a self-integrating loop (SIL)-type sensor has been built. These sensors have been characterised using TDR techniques for their risetime as well as surge impedance.

For the measurement of the voltage, noninductive-type resistance divider with a response time of 5.2 ns (within the working volume) has been built. As the height of the HV electrode of the illuminator is the same as its width at any point along the axis, the antenna behaves as a very good shield for the resistive voltage divider or, in other words, the voltage divider behaves like a field-controlled resistive divider where the effect of the stray capacitances is nonexistent.

4. Summary

A parallel plate EMP simulator of working volume $5 \times 5 \times 5$ mm, surge impedance 150 Ω and resonant frequency 120 MHz has been developed and successfully tested. Voltage waveform measurements have been carried out in the working volume and the voltage waveform was found to have an acceptable risetime of 10.3 ns and duration of 262 ns (Fig. 4). Also electric and magnetic field sensors have been developed and characterised for this impedance and risetime. Their performance has been found to be satisfactory.

References

1. GLASSTONE, S. AND DOLAN, P. J. *The effects of nuclear weapons*, 3rd edition, 1980, Castle House.

2. HILL, J. S. Electromagnetic compatibility technology applied to the nuclear electromagnetic pulse, *Proc. Int. Symp. on EMC*, New York, 1973, pp. 3–11.

3. *EMP engineering and design principles*, 1975, Bell Telephone Laboratories, Inc., Whippany, NJ.

4. LEE, K. S. H. (ED.) *EMP interaction: Principles, techniques and reference data*, 1986, Hemisphere.

5 DEB, G. K. An indian view of nuclear electromagnetic pulse protection policy, *Electromagnetic Compatibility J.*, 1988, **1**, 54–63.

6. Special issue on nuclear electromagnetic pulse, *IEEE Trans.*, Feb. 1978, **EMC-20**.

Thesis Abstract (Ph. D.)

Behaviour of expansive soils cushioned with stabilized rice husk ash and a critical appraisal of CNS soil as a cushion by J. V. Gurumurthy

Research supervisors: K. S. Subba Rao and P. V. Sivapullaiah
Department: Civil Engineering

1. Introduction

One of the most challenging tasks for the geotechnical engineers is to protect structures from distress caused by expansive soils. According to a survey[1], the amount spent every year in America alone, in rectifying the damages caused by expansive soils, is $2,255 m. Among several methods available to counter the ill effects of expansive soil, one is providing a cushion between the foundation and soil. The cushion material was obviously nonexpansive, and early studies with sand showed marginal improvement. Subsequent studies by Katti and Kulkarni[2] using a cohesive nonswelling (CNS) soil as a cushion material showed much better promise. The use of CNS as a cushion material has been widely accepted in India. Some specifications as to what constitutes a CNS material, the placement conditions and the thickness to be provided, have been given by Katti[3], based on his experience. The applicability of CNS material as a cushion has never been examined in the light of the cyclic behaviour. There are very few field records showing the behaviour of CNS-treated foundations. Also what is not clear is how reliable or rigorous the specifications are with regard to the CNS material. Further, the placement of CNS material at its Proctor optimum conditions calls for strict quality control, which often is not ensured.

The thesis examines the behaviour of expansive soil, cushioned with either standard or nonstandard CNS material, not only during the first wetting, but also during subsequent cycles of wetting and drying. A brief presentation is made of the methods available for identification and classification of expansive soil and the field heave measurements reported in literature are summarized.

2. Results and discussion

Detailed studies on the expansive characteristics of black cotton (BC) soil and bentonite have been carried out. The behaviour of these soils, when cushioned with a standard or nonstandard CNS soil layer, is also studied over the first cycle of wetting. One nonstandard CNS material, [CNS(NS1)], had higher clay content of 38% than the specified maximum clay content of 20%. The other nonstandard CNS soil, [CNS(NS2)], had a higher sand content of 55% than the speci-

fied maximum sand content of 35%. Based on the oedometer swelling and consolidation tests conducted over expansive soil–CNS systems, it has been shown that CNS soil cushion is effective in reducing the per cent swell, swelling pressure, compression index, coefficient of volume change and in increasing the coefficient of consolidation of expansive soil. The effect of cushion increases with increase in the cushion thickness ratio and cohesion. Further, it is noticed that the effect of cushion is more pronounced at lower surcharges. The studies further bring out that the specifications for CNS soil given by Katti[3] are not rigorous. In fact, CNS(NS1) having higher clay content, is more advantageous than CNS itself. However, CNS(NS2), having higher sand content, is less effective. This underlies the importance of cohesion of cushion material.

Expansive soils, over their active zone, invariably undergo cyclic swelling and shrinkage. While full swelling can occur with continuous rainfall during the rainy season (June to October), full shrinkage is unlikely to take place, because the process of shrinkage takes a very long time. So the experiments were aimed at the study of the cyclic swell–shrink behaviour of both expansive and CNS-cushioned expansive soils, under two conditions: full swelling and full shrinkage cycles, full swelling and partial shrinkage cycles. Cyclic tests are continued till the equilibrium bandwidth of vertical movements (swell–shrink movements) is reached.

The thesis clearly brings out a matter of great concern, in that the CNS materials, both standard and nonstandard, become totally ineffective during the swell–shrink cycles. The reason is not difficult to find. Though these compacted CNS soils do not swell in the first cycle of wetting, they can shrink. Once shrunken, they can swell. In other words, they do not remain cohesive, nonswelling materials from their shrunken levels.

A search for an effective cushion material, which neither swells nor shrinks, but has other properties like cohesion, strength and good permeability was therefore made. The thesis presents such a material. Rice husk ash (RHA), which is abundantly available, has been explored for its use as a cushion material. Its poor cohesion is improved with the addition of 6% lime or cement. The chapter contains the properties of RHA and that of stabilized RHA.

The thesis is also devoted to the study of expansive and compressibility characteristics of BC soil, when cushioned with lime-stabilized RHA (LSR) or cement-stabilized RHA (CSR). The results show that the use of stabilized RHA as a cushion, reduces the swelling and swelling pressure of expansive soil. The higher the cushion thickness ratio or surcharge, the higher is the reduction. Further, the consolidation characteristics of expansive soil, like C_c, C_s, m_v and c_v are improved. The efficiency increases with increase in the cushion thickness ratio. The differences in the effects of LSR and CSR on the swelling and consolidation properties of soils are negligible. The results presented in this chapter establish that both LSR and CSR are not only effective in the first cycle of swelling, but also during subsequent cycles of swelling and shrinkage.

A comparative analysis of performances of different cushion materials has been done throughout this thesis. It has been shown that LSR or CSR is distinctly superior to CNS soil as a cushion in controlling the properties of expansive soils. Illustrative examples of heave computations have been made for strip and square footings, to demonstrate, in quantitative terms, the improved behaviour of stabilized RHA as a cushion.

3. Conclusions

From the results reported in this thesis, the following conclusions are drawn:

1. Cohesive nonswelling (CNS) soil as a cushion is effective in reducing the per cent swell, swelling pressure, compression index, coefficient of volume change and in increasing the coefficient of consolidation of expansive soil. All these changes occur during the first wetting of the

expansive soil. The effect of cushion increases with increase in the cushion thickness ratio. Greater the density (or cohesion) of the cushion, more effective is the cushion in reducing the swelling. The effect of CNS soil cushion is higher at lower surcharges.

2. The available tentative specifications for CNS soil are not rigorous, and deviations towards increased clay content (cohesion) are advantageous. But, on the other hand, a CNS soil containing higher sand content than specified is less effective as a cushion material.

3. The potential for volumetric change in a BC–CNS system is about the same as that of BC soil, in the long run; if anything, slightly worse. The CNS soil cushion is ineffective during both full swelling–full shrinkage and full swelling–partial shrinkage cycles.

4. The effect of surcharge does not bring any qualitative change in the swell–shrink behaviour of expansive soil irrespective of the type of CNS cushion material. However, the magnitudes of operating movement levels are lowered with increase in the surcharge.

5. Rice husk ash (RHA) stabilized with lime or cement develops properties required for a cushion material, like strength, good permeability, low compressibility, and insignificant swelling and shrinkage. RHA stabilized with either 6% lime or 10% cement is generally considered adequate for application as a cushion material.

6. The use of stabilized RHA as a cushion, reduces the swelling and swelling pressure of expansive soils. This is so not only in the first cycle of swelling, but also during subsequent cycles of swelling and shrinkage. The swelling potential of the soil decreases with increasing cushion thickness ratio. The efficiency of LSR or CSR in reducing the swelling potential increases with increase in the surcharge.

7. The differences in the effects of LSR and CSR on the swelling and consolidation properties of soils are negligible.

8. From all the swelling and consolidation characteristics studied, the behaviour of BC–LSR or BC–CSR is distinctly superior to that of a BC–CNS system.

References

1. CHEN, F. H. — *Foundations on expansive soils*, 1975, Elsevier.

2. KATTI, J. M. AND KULKARNI, S. K. — Studies on non-swelling soil layer as a means to resist swelling pressure of expansive soil system, *South East Asian Regional Conf. on Soil Engineering*, Bangkok, 1967, pp. 147–157.

3. KATTI, R. K. — First IGC annual lecture-search for solutions to problems in black cotton soils, *Indian Geotech. J.*, 1979, **9**, 1–80.